

The effect of electric-field-induced alignment on the electrical mobility of fractal aggregates

James Corson, George W. Mulholland & Michael R. Zachariah

To cite this article: James Corson, George W. Mulholland & Michael R. Zachariah (2018): The effect of electric-field-induced alignment on the electrical mobility of fractal aggregates, Aerosol Science and Technology, DOI: [10.1080/02786826.2018.1427210](https://doi.org/10.1080/02786826.2018.1427210)

To link to this article: <https://doi.org/10.1080/02786826.2018.1427210>

 View supplementary material 

 Accepted author version posted online: 16 Jan 2018.
Published online: 30 Jan 2018.

 Submit your article to this journal 

 Article views: 17

 View related articles 

 View Crossmark data 



The effect of electric-field-induced alignment on the electrical mobility of fractal aggregates

James Corson^a, George W. Mulholland^a, and Michael R. Zachariah^{a,b}

^aDepartment of Chemical and Biomolecular Engineering, University of Maryland, College Park, Maryland, USA; ^bDepartment of Chemistry and Biochemistry, University of Maryland, College Park, Maryland, USA

ABSTRACT

We study the effects of electric field strength on the mobility of soot-like fractal aggregates (fractal dimension of 1.78). The probability distribution for the particle orientation is governed by the ratio of the interaction energy between the electric field and the induced dipole in the particle to the energy associated with Brownian forces in the surrounding medium. We use our extended Kirkwood–Riseman method to calculate the friction tensor for aggregates of up to 2000 spheres, with primary sphere sizes in the transition and near-free molecule regimes. Our results for electrical mobility versus field strength are in good agreement with published experimental data for soot, which show an increase in mobility on the order of 8% from random to aligned orientations. Our calculations show that particles become aligned at decreasing field strength as particle size increases because particle polarizability increases with volume. Large aggregates are at least partially aligned at field strengths below 1000 V/cm, though a small change in mobility means that alignment is not an issue in many practical applications. However, improved differential mobility analyzers would be required to take advantage of small changes in mobility to provide shape characterization.

ARTICLE HISTORY

Received 5 October 2017
Accepted 3 January 2018

EDITOR

Yannis Drossinos

1. Introduction

The transport behavior of nanoscale particles depends on particle size, shape, and orientation. In the absence of an external field, Brownian motion randomizes the particle orientation, such that the measured transport property (e.g., intensity of scattered light, particle mobility) represents an average over all equally likely particle orientations. In a strong field, particles become aligned in an orientation that minimizes their energy in the field (Fuchs 1964; Li et al. 2014a). This effect has been demonstrated experimentally by placing particles in an external electric field and measuring changes in scattered light intensity (Weiss et al. 1992; Colbeck et al. 1997) or electrical mobility (Kousaka et al. 1996; Zelenyuk and Imre 2007; Li et al. 2012, 2016) as the field strength changes.

One common experimental technique for sizing nanoparticles involves using a differential mobility analyzer (DMA) to determine the mobility of particles in an electric field. The particle transport behavior is often expressed in terms of the mobility diameter, which is the

diameter of a sphere that has the same mobility as that of the particle. For spherical particles, the measured mobility diameter is equal to the geometric diameter and is independent of field strength. However, for nonspherical particles, the mobility is a function of field strength. Plots of mobility *versus* field strength are typically S-shaped, with the lower plateau at low fields representing fully random particle orientation and the upper plateau at high fields representing fully aligned orientation (Kousaka et al. 1996; Zelenyuk and Imre 2007; Li et al. 2012, 2016). The increase in mobility (decrease in drag and mobility diameter) with increasing field strength is due to the electrical polarizability of the particles. This means that particles tend to align such that the longest particle dimension is parallel to the electric field. For example, a long, thin rod orients its long axis parallel to the electric field direction at high field strengths.

Researchers have proposed experimental methods for obtaining shape information or separating particles with different shapes by exploiting the dependence of particle mobility on orientation in a DMA (Zelenyuk and Imre

CONTACT Michael R. Zachariah ✉ mrz@umd.edu Department of Chemical and Biomolecular Engineering, University of Maryland, 4418 Stadium Dr., College Park, MD 20742, USA.

Color versions of one or more of the figures in the article can be found online at www.tandfonline.com/uast.

Supplemental data for this article can be accessed on the [publisher's website](#).

2007; Li et al. 2014b, 2016). Such procedures involve size-selecting particles in consecutive DMAs operated at different field strengths (or, equivalently, at different sheath flow rates). The observed change in mobility may give some clues about the shape of particles in the tandem DMAs.

The present study applies the theory of Li et al. (2014a) for the average particle mobility as a function of field strength to calculate the mobility of aggregates with a fractal dimension of 1.78, which is characteristic of soot and other particles formed by diffusion-limited cluster aggregation (DLCA). In the present study, we apply our extended Kirkwood–Riseman (EKR) method (Corson et al. 2017a) to obtain the translational friction tensor that appears in the theory of Li et al. (Li et al. 2012, 2014a). We compare our results to experimental data (Li et al. 2016) and show how the particle mobility changes with electric field strength for a wide range of primary sphere diameters and aggregate sizes. We also use our EKR method to estimate the particle rotational relaxation time (Corson et al. 2017d) to evaluate the range of particle sizes for which it is appropriate to apply the orientationally averaged drift velocity method of Li et al. (2014a) to compute particle mobility. Finally, we discuss the implications of our results for obtaining shape information by measuring the effect of electric field strength on particle mobility.

2. Theoretical methods

Before discussing our theoretical methods in detail, we will provide an overview of its various components. First, we compute the velocity field and the monomer friction coefficient as a function of Knudsen number by solving the Bhatnagar–Gross–Krook (BGK) model equation (Bhatnagar et al. 1954) using the method of Loyalka and colleagues (Lea and Loyalka 1982; Law and Loyalka 1986). The BGK equation is a simplified, linearized version of the Boltzmann transport equation, valid for near-equilibrium situations such as creeping flow of a sphere. This is done once for each Knudsen number, with the velocity results saved for future use.

The second component involves computing the friction tensor for a cluster of monomers by self-consistent computing of the flow field at each monomer resulting from the flow field arising from all the other monomers (Corson et al. 2017a). The low density of the aggregates is key to carrying out the calculations of large clusters in a short time. This approach was initially used by Kirkwood and Riseman (1948) for computing the friction tensor for macromolecules in continuum flow. By using the BGK results for the flow field in the transition regime, we can compute

the friction tensor of clusters composed of equal sized monomer units. We have also applied the theory to determine the rotational friction tensor (Corson et al. 2017c), which is necessary for assessing the possible effect of rotation on the mobility.

Another element of the analysis is the calculation of the cluster polarizability tensor, which is needed for computing the potential energy associated with alignment. We have obtained the polarizability tensor for the aggregates in this study from ZENO (Mansfield et al. 2001), which uses a random walk algorithm (Douglas et al. 1994) to compute (among other things) the polarizability tensor for a perfectly conducting particle of arbitrary shape. We assume that aggregate particles (e.g., soot) are perfectly conducting.

The final element involves the matrix manipulations and the ensemble averaging (Happel and Brenner 1965; Li et al. 2014a) to obtain the drift velocity (mobility) in the direction of the electric field.

We now discuss the theory in more detail in the following sections.

2.1. Particle orientation in an electric field

The probability distribution of a particle's orientation in an electric field is given by the Boltzmann distribution (Fuchs 1964),

$$f(\varphi, \theta, \psi) = \frac{e^{-U/kT}}{\int_0^{2\pi} \int_0^{\pi} \int_0^{2\pi} e^{-U/kT} \sin\theta \, d\varphi \, d\theta \, d\psi} \quad [1]$$

where U is the energy of the particle in the electric field for the particle orientation given by the Euler angles (φ, θ, ψ) . This equation shows that the probability distribution is affected by the competition between randomizing Brownian forces from collisions of gas molecules with the particle, and electrical forces that tend to align the particle in a particular direction. For nonpolar materials, the interaction energy includes contributions from free charges on the particle and from an induced dipole due to polarization in the electric field (Bottcher and Belle 1973). The interaction energy from a fixed charge is

$$U_e = -q\vec{r}_e \cdot \vec{E} \quad [2]$$

where \vec{r}_e is the vector from the center of mass to the point charge and \vec{E} is the electric field. For a conducting particle, the interaction energy from an induced dipole

is given by (Bottcher and Belle 1973)

$$U_p = -\frac{1}{2}\vec{E}\cdot\alpha\cdot\vec{E} \quad [3]$$

where α is the electrical polarizability tensor. According to Fuchs (1964), aerosol particles can be assumed to be conductors, even when comprised of nonconducting materials, due to the presence of surface contaminants.

$$\mathbf{A} = \begin{bmatrix} \cos\varphi\cos\psi - \cos\theta\sin\varphi\sin\psi & -\cos\varphi\sin\psi - \cos\theta\sin\varphi\cos\psi & \sin\varphi\sin\theta \\ \sin\varphi\cos\psi + \cos\theta\cos\varphi\sin\psi & -\sin\varphi\sin\psi + \cos\theta\cos\varphi\cos\psi & -\cos\varphi\sin\theta \\ \sin\psi/\sin\theta & \cos\psi/\sin\theta & \cos\theta \end{bmatrix} \quad (5)$$

From Equations (2) and (3), the free charge and induced dipole interaction energies increase linearly and quadratically, respectively, with electric field strength. Furthermore, the charge interaction energy increases linearly with particle characteristic length, while the induced dipole interaction energy increases linearly with particle volume. Because the polarization energy increases with a^3 , while the charge energy increases with a , and because the particle orientation depends on the Boltzmann factor $e^{-U/kT}$, we can often ignore the effects of point charges when computing the probability distribution for the particle's orientation. For example, Li et al. (2012) determined that the ratio of polarization energy to fixed charge energy is greater than 10 for carbon nanotubes with mobility diameters greater than 100 nm, while Zelenyuk and Imre (2007) observed no effects of particle charge on the mobility of aligned doublets with primary sphere diameters of 240 nm. Also, for a conducting particle the charge can move rapidly, so that one can consider the charge to be distributed evenly throughout the particle (Bottcher and Belle 1973). Based on these considerations, we will consider only the polarization energy when computing the particle mobility.

To evaluate the probability distribution (Equation (1)), it helps to define two coordinate systems: a body-fixed coordinate system (x', y', z') that rotates with the particle, and a space-fixed (or laboratory) coordinate system (x, y, z) (see the online supplementary information [SI]). For convenience, we will choose the body-fixed axes to coincide with the principal axes of the polarizability tensor. In this representation, the minimum polarization energy occurs when the electric field is along the z' -direction. We will set our space-fixed axes so that the z -axis is parallel to the electric field.

The relationship between a vector in laboratory coordinates and a vector in body-fixed coordinates is given

by the following relationship:

$$\vec{b} = \mathbf{A}\cdot\vec{b}' \quad [4]$$

The rotation matrix \mathbf{A} represents three successive rotations from the body-fixed system to the space-fixed system. For the ZXZ sequence of rotations, the rotation matrix is given by

where φ , θ , and ψ are the angles of the first, second, and third rotations, respectively. One useful property of the rotation matrix is that its inverse is equal to its transpose (Gel'fand et al. 1963). Because of this property and our choice of laboratory coordinates, the electric field in body-fixed coordinates is given by

$$\vec{E}' = \begin{bmatrix} \sin\psi/\sin\theta \\ \cos\psi/\sin\theta \\ \cos\theta \end{bmatrix} E \quad [6]$$

where E is the field strength. This shows that the probability distribution is a function of only two of the three Euler angles. Using the above expression for the electric field and noting that the polarizability tensor in body-fixed coordinates is diagonal, we can explicitly write the interaction energy as

$$U = -\frac{1}{2}(\sin^2\psi\sin^2\theta\alpha_1 + \cos^2\psi\sin^2\theta\alpha_2 + \cos^2\theta\alpha_3)E^2 \quad [7]$$

where $\alpha_3 > \alpha_2 > \alpha_1$ are the eigenvalues of the polarizability tensor.

2.2. Average drift velocity of a particle in an electric field

We can use the probability distribution in Equation (1) to calculate the average drift velocity—and thus the mobility—of a particle in an electric field (Li et al. 2014a). The drift velocity is obtained by balancing the electric force on the particle with the aerodynamic force

for a given particle orientation:¹

$$\vec{V}_d = q\Xi_t^{-1} \cdot \vec{E} \quad [8]$$

Here, Ξ_t is the translational friction tensor and q is the charge on the particle. Combining Equations (1) and (8), we get the following expression for the particle orientation-averaged drift velocity for a given electric field strength:

$$\langle \vec{V}_d \rangle = \frac{q \int_0^{2\pi} \int_0^{\pi} \int_0^{2\pi} (\Xi_t^{-1} \cdot \vec{E}) e^{-U/kT} \sin\theta \, d\varphi \, d\theta \, d\psi}{\int_0^{2\pi} \int_0^{\pi} \int_0^{2\pi} e^{-U/kT} \sin\theta \, d\varphi \, d\theta \, d\psi} \quad [9]$$

In general, the orientation-averaged drift velocity is not parallel to the electric field. However, the component of the drift velocity parallel to the electric field is typically much larger than the components of the velocity perpendicular to the field. For example, the perpendicular components of the drift velocity for soot-like fractal aggregates are typically less than 5% of the parallel component. Thus, we can define the particle mobility in terms of the parallel component of the orientation-averaged drift velocity.

$$Z = \langle V_{d,z} \rangle / E \quad [10]$$

Again, we have positioned the laboratory-fixed coordinate system so that the electric field is in the z -direction. The z -component of the drift velocity can be written in terms of the Euler angles and the components of the friction tensor in body-fixed coordinates:

$$\begin{aligned} \langle V_{d,z} \rangle = & qE (M_{33} \langle \cos^2\theta \rangle + M_{22} \langle \cos^2\psi \sin^2\theta \rangle \\ & + M_{11} \langle \sin^2\psi \sin^2\theta \rangle + M_{12} \langle \sin 2\psi \sin^2\theta \rangle \\ & + M_{13} \langle \sin\psi \sin 2\theta \rangle + M_{23} \langle \cos\psi \sin 2\theta \rangle) \end{aligned} \quad [11]$$

Here, the angle brackets indicate orientation averages based on the distribution given by Equation (1) and the M_{ij} 's are components of the mobility tensor (i.e., the inverse of the friction tensor) in body-fixed coordinates,

i.e.,

$$\mathbf{M} \equiv \begin{bmatrix} M_{11} & M_{12} & M_{13} \\ M_{12} & M_{22} & M_{23} \\ M_{13} & M_{23} & M_{33} \end{bmatrix} = (\Xi_t')^{-1} \quad [12]$$

In going from Equation (9) to Equation (11), we use the relation between the body-fixed (Ξ_t') and space-fixed (Ξ_t) friction tensors, $\Xi_t^{-1} = \mathbf{A} \cdot (\Xi_t')^{-1} \cdot \mathbf{A}^\dagger$, where the dagger symbol denotes the transpose of the rotation matrix. Note that Equation (11) reduces to the expressions given by Li et al. (2012) for the special case of an axisymmetric body, where $M_{12} = M_{13} = M_{23} = 0$, $M_{11} = M_{22} = M_\perp$, and $M_{33} = M_\parallel$.

For a randomly oriented particle, the averaged mobility is

$$Z_{rand} = \frac{q}{3} \left(\frac{1}{\zeta_1} + \frac{1}{\zeta_2} + \frac{1}{\zeta_3} \right) \quad [13]$$

where $\zeta_1 > \zeta_2 > \zeta_3$ are the eigenvalues of the translational friction tensor. At very high field strengths, the particle will be oriented in the direction that minimizes the electric field interaction energy. Thus, the high-field mobility is

$$Z_{align} = q \hat{k} \cdot (\Xi_t')^{-1} \cdot \hat{k} = qM_{33} \quad [14]$$

where \hat{k} is the unit vector in the z -direction.

2.3. Friction tensor for an aggregate

To calculate the orientation-averaged mobility of soot-like particles, we must be able to determine the translational friction tensor for fractal aggregates consisting of N primary spheres with radius a , where the Knudsen number of the primaries ($\text{Kn} = \lambda/a$) is in the transition regime between continuum ($\text{Kn} \ll 1$) and free molecule ($\text{Kn} \gg 1$) limits. To do so, we will use our extension (Corson et al. 2017a) of Kirkwood–Riseman theory (Kirkwood and Riseman 1948) from the continuum regime to the transition regime.

Kirkwood and Riseman (1948) proposed a method for calculating the translational friction coefficient for a macromolecule or particle consisting of spherical subunits. The drag on each sphere in the aggregate is obtained by considering the effects of the other spheres in the particle on the flow field. The resulting force is the sum of the drag on an isolated particle

¹The linear relationship between the velocity and the drag force is valid in the creeping flow regime, which applies for all of the conditions considered in this study.

and the perturbations due to the other spheres:

$$\vec{F}_i = -\zeta_0 \vec{U}_i - \zeta_0 \sum_{i \neq j}^N \vec{T}_{ij} \cdot \vec{F}_j \quad [15]$$

Here, $\zeta_0 = 6\pi\mu a$ is the friction coefficient for a sphere given by Stokes' law, \vec{U}_i is the velocity of the i th sphere, and \vec{T}_{ij} is the hydrodynamic interaction tensor. Carrasco and Garcia de la Torre (1999) discuss some of the hydrodynamic interaction tensors that have been proposed in the past and the relative accuracy of the various forms of \vec{T}_{ij} . They conclude that the Rotne–Prager–Yamakawa (RPY) tensor (Rotne and Prager 1969; Yamakawa 1970)—which is accurate to order r_{ij}^{-3} , where r_{ij} is the distance between spheres—is sufficiently accurate for practical purposes.

Noting that the product of the RPY tensor and the monomer friction coefficient is similar to the tensor \vec{V}_{ij} describing the flow field around a sphere moving with velocity \vec{U}_i (i.e., $\vec{u}(r_{ij}) = \vec{V}_{ij} \cdot \vec{U}_i$), we proposed replacing $\zeta_0 \vec{T}_{ij}$ with $\vec{V}_{ij}(\text{Kn})$, the velocity field around a moving sphere in the transition flow regime (Corson et al. 2017a):

$$\vec{F}_i = -\zeta_0(\text{Kn}) \vec{U}_i - \sum_{i \neq j}^N \vec{V}_{ij}(\text{Kn}) \cdot \vec{F}_j \quad [16]$$

This EKR approach is valid for creeping flow for any Knudsen number, provided one can accurately solve for the velocity field around a sphere as a function of Kn.

We obtain the velocity field and the monomer friction coefficient that appear in Equation (16) by solving the BGK model equation (Bhatnagar et al. 1954) using the method of Loyalka and colleagues (Lea and Loyalka 1982; Law and Loyalka 1986). The BGK equation is a simplified, linearized version of the Boltzmann transport equation, valid for near-equilibrium situations such as creeping flow of a sphere. We solve Equation (16) for unit particle velocity in the x -, y -, and z -directions to determine the translational friction tensor. Our EKR results for the translational friction coefficient of fractal aggregates compare well to published experimental data and calculational results (Corson et al. 2017a,b).

3. Results

To determine the orientation-averaged mobility of fractal aggregates, we solve Equation (11) with the translational friction tensor calculated using our EKR method

and the polarizability tensor [which appears in the potential energy term, Equation (7), that affects particle orientation] obtained from ZENO (Mansfield et al. 2001). ZENO uses a random walk algorithm (Douglas et al. 1994) to compute (among other things) the polarizability tensor for a perfectly conducting particle of arbitrary shape. Again, we assume that soot particles are perfectly conducting. The polarizability and friction tensors are specified in terms of the body-fixed axes, which correspond to the principal axes of the polarizability tensor, as discussed previously. We obtain the orientation averages in Equation (11) by integrating numerically using a 2D quadrature method (MATLAB function integral 2). We generate our aggregates using a cluster-cluster algorithm (Mackowski 2006). For each N , we generate 20 clusters and present the average results of the 20 cases.

3.1. Comparison to experimental data

Li et al. (2016) used a pulsed-field differential mobility analyzer (PFDMA) to determine the electrical mobility of soot aggregates composed of 5-nm-radius primaries (Kn = 13.5 for $\lambda = 67.3$ nm). They size-selected aggregates with mobility diameters of approximately 129, 154, and 200 nm in a DMA operated at high field (~ 7000 – 8000 V/cm), then used the PFDMA to measure the mobility of these aggregates as a function of electric field strength.

For our calculations, we must first estimate the aggregate size and structure from the reported mobilities. Like Li et al. (2016), we assume that the aggregates have a fractal morphology,

$$N = k_0 \left(\frac{R_g}{a} \right)^{d_f} \quad [17]$$

with fractal dimension $d_f = 1.78$ and prefactor $k_0 = 1.3$. We determine the number of primaries iteratively until we obtain a set of particles whose average random mobility (as calculated using our EKR method) is in good agreement with the experimental mobility at low field. We repeat this procedure for the three data sets, corresponding to mobility diameters of 129, 154, and 200 nm. As an initial guess for N , we solve for N in our expression for the friction coefficient of DLCA aggregates (Equation (38) of (Corson et al. 2017b)):

$$\frac{\zeta}{6\pi\mu a} = \frac{1 + 1.612\text{Kn}}{C_c(\text{Kn})} \left\{ [0.852N^{0.535} + 0.148]^{-1} + 1.612\text{Kn} [0.843N^{0.939} + 0.157]^{-1} \right\}^{-1} \quad [18]$$

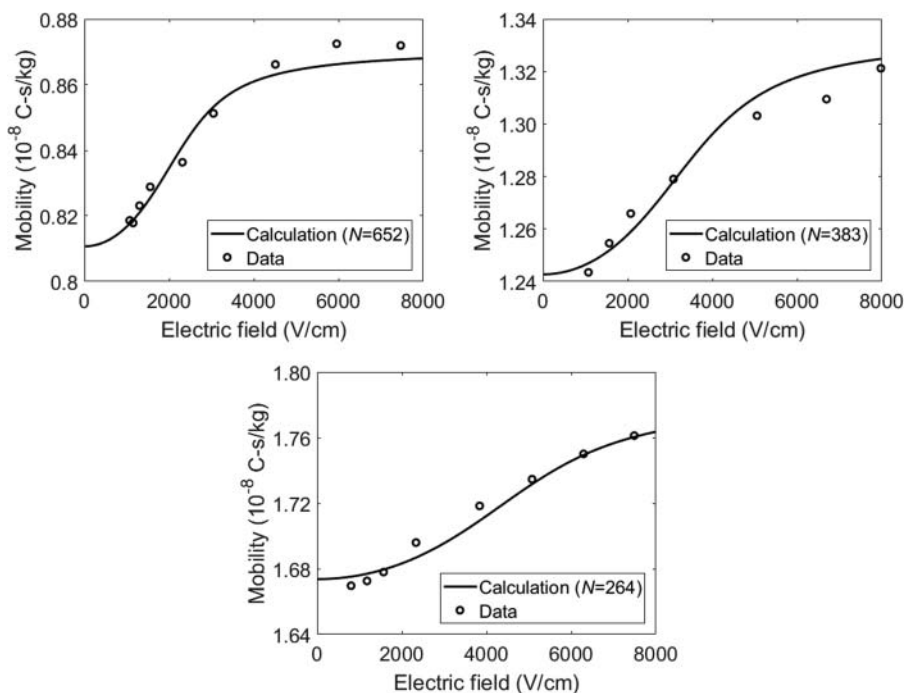


Figure 1. Comparison of our calculated orientation-averaged mobilities to experimental data from Li et al. (2016) for mobility diameters of ~ 129 nm, ~ 154 nm, and ~ 200 nm (based on the high-field mobilities). The number of primaries used for the calculations represent the best fits to the data.

The friction coefficient is related to the mobility by $\zeta = q/Z$.

Figure 1 compares the results of our calculations to data from Li et al. (2016). Overall, the results are in good agreement with the data, enabling us to consider a parametric study outside the bounds of available experimental data.

3.2. Effects of aggregate size and field strength on mobility

Now that we have shown that the theory of Li et al. (2014a) used in concert with our EKR method can be used to calculate the orientation-averaged mobility of soot as a function of electric field strength, we will use this approach to calculate the mobility of DLCA aggregates over a wider range of primary spheres and aggregate sizes. Again, our mobility results represent the average of 20 realizations from our fractal generator. Our calculations assume that Brownian rotation is slow compared to the translational relaxation time of the particles. This means that the drag force and the electric force are immediately balanced at each particle orientation. Mulholland et al. (2016) show the slow rotation limit applies for reduced rotational velocity $\alpha_{nr} = 2D_{r,\min}\tau_t < 0.05$. Here, $\tau_t = m/\zeta_h$ is the translational relaxation time, ζ_h is the translational friction coefficient computed as the harmonic mean of the eigen-

values of the translational friction tensor, m is the particle mass, and $D_{r,\min}$ is the rotational diffusion coefficient of the particle about the axis that yields the minimum D_r . We will examine the validity of this assumption in Section 4.

Figure 2 shows the effect of electric field strength on the normalized mobility Z/Z_{rand} of $N = 100$ and $N = 1000$ aggregates at Knudsen numbers corresponding to primary sphere radii of 25 nm ($Kn = 2.7$), 13.5 nm ($Kn = 5$), 9.6 nm ($Kn = 7$), 6.7 nm ($Kn = 10$), and 5 nm ($Kn = 13.5$). Particles become aligned at lower electric fields as the primary size and the number of primaries increase. For $N = 1000$, particles are fully aligned at fields as low as approximately 500 V/cm for the 25 nm primaries *versus* approximately 5000 V/cm for the 5 nm primaries. The physical basis of this result will be discussed later in the article. The normalized fully aligned mobility for the 1000-sphere aggregates increases slightly with decreasing Knudsen number (increasing primary radius). The maximum increase in mobility from random orientation to fully aligned is approximately 8%.²

Figure 3 shows normalized mobility *versus* electric field strength for $Kn = 2.7$ and $Kn = 13.5$ at various aggregate sizes. All but the smallest aggregates

²For comparison, the change in the intensity of scattered light between aligned and random states has been demonstrated to be as large as $\sim 50\%$ for soot (Weiss et al. 1992; Colbeck et al. 1997).

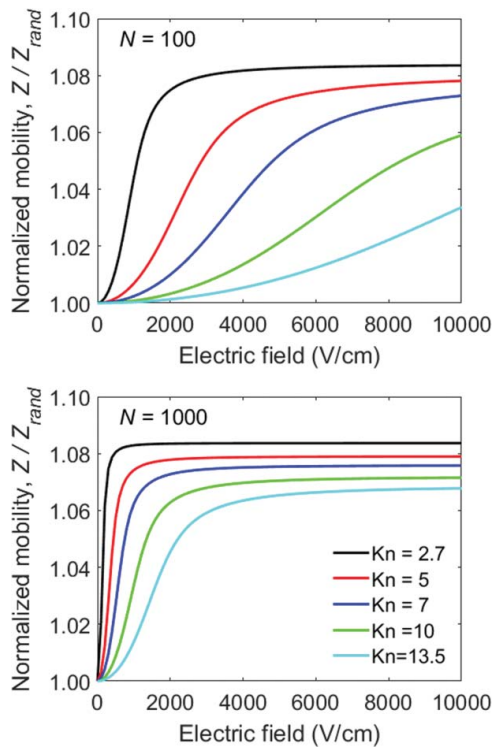


Figure 2. Normalized mobility as a function of electric field strength for 100-sphere (top) and 1000-sphere (bottom) aggregates.

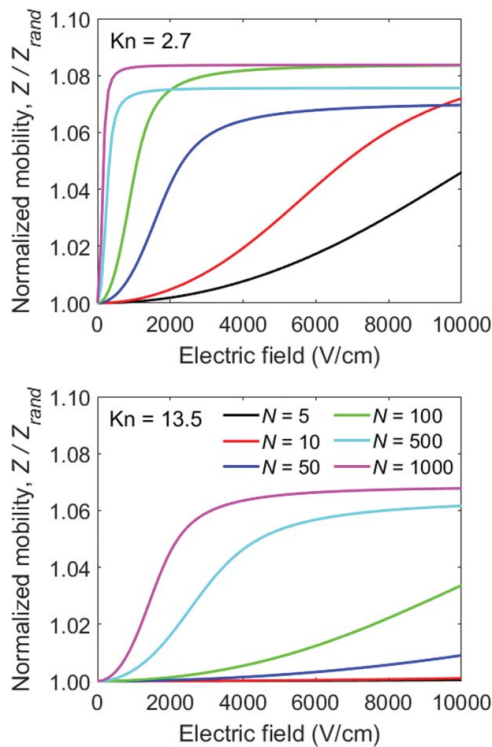


Figure 3. Normalized mobility as a function of electric field strength for aggregates with primary sphere radii of 25 nm ($Kn = 2.7$, top) and 5 nm ($Kn = 13.5$, bottom). Note that the $N = 100$ and $N = 1000$ curves in this figure correspond to the $Kn = 2.7$ and $Kn = 13.5$ curves in Figure 2.

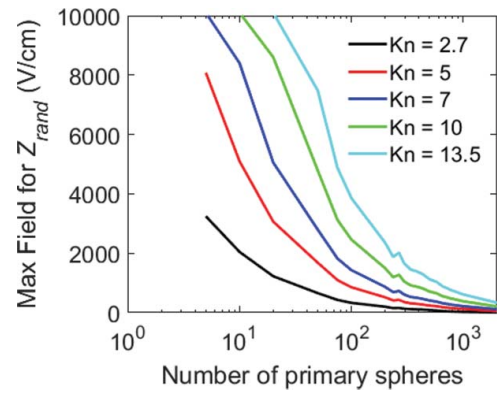


Figure 4. Maximum electric field strength at which particles are randomly oriented, defined as having a mobility within 0.5% of the mobility in the limit of zero-field strength. Note that results are capped at an upper limit of $E = 10,000$ V/cm.

with 25 nm radius primaries ($Kn = 2.7$) are fully aligned at 8000 V/cm, while only the larger aggregates with 5 nm radius primaries ($Kn = 13.5$) are fully aligned at this field strength. The latter point is consistent with the data of Li et al. (2016) and our results shown in Figure 1. Note that several of the lines in the $Kn = 2.7$ plot cross each other. This is due to statistical variations in the fully aligned mobility, caused by the finite number of particles we use to generate the results for each N . We will return to this issue in the final paragraph of this section.

From Figures 2 and 3, it is clear that particle orientation may not be fully random even at low field strengths. It is useful to determine the maximum field at which the particle orientation is random; we show this maximum field as a function of N and Kn in Figure 4. Here, we

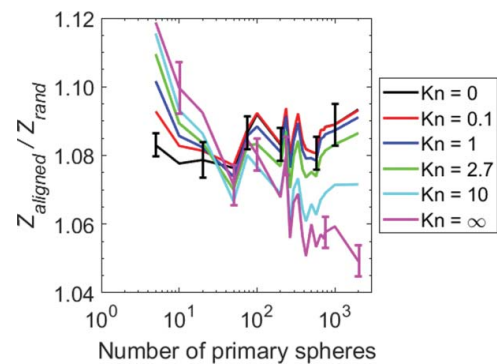


Figure 5. Ratio of fully aligned to random electric mobilities for a wide range of primary sphere Knudsen numbers and the number of primaries. The $Kn = 0$ and $Kn = \infty$ curves represent the continuum and free molecule limits, as calculated using the standard KR theory with the RPY tensor (Chen et al. 1984) and using a Monte Carlo code (Corson et al. 2017c), respectively. Uncertainties of one standard deviation of the mean (based on 20 samples with the same fractal dimension but different morphologies) are shown for the continuum and free molecule results for several N values.

consider the particle orientation to no longer be random when the mobility increases by 0.5% from the mobility in the limit of zero field. Again, particles begin to partially align at lower field strengths as particle size (both N and a) increase.

Finally, Figure 5 shows the mobility ratio, Z_{align} / Z_{rand} , as a function of N for several Knudsen numbers. The random and fully aligned mobilities are calculated using Equations (13) and (14), respectively. Generally speaking, the mobility ratio is constant with increasing N near the continuum regime and decreases with N in the free molecule regime. At intermediate Knudsen numbers, the aligned *versus* random behavior becomes more continuum-like at large N ; this is analogous to the behavior we have observed for the translational friction coefficient of soot-like aggregates (Corson et al. 2017b). We will explain this behavior in Section 4. Note that each point in the figure represents an average over 20 particle realizations. To give an idea of the uncertainty in the mean values shown in the figure, we show bounds of one standard deviation of the mean for several N 's in the continuum and free molecule limits. See the SI for further discussion about the variability in the mobility ratio results.

The choppiness in the plots in Figure 5 can be explained by the statistics of our results: the standard deviation of Z_{align} / Z_{rand} is approximately 0.03 for all cases, and thus the standard deviation of the mean³ is approximately 0.007. Assuming our samples are normally distributed about the population mean, we would expect 68% of our samples to be within one standard deviation of the population mean. Indeed, most of the mean mobility ratios for $Kn = 0, 0.1,$ and 1 are within 0.007 of an estimated population mean of 1.085, so it is reasonable to conclude that the spread in Z_{align}/Z_{rand} is partially due to our finite sample size.

4. Discussion

4.1. General observations

Our results show that particle alignment occurs at decreasing electric field strengths as the primary sphere Knudsen number decreases (primary sphere radius increases) and as the number of primaries increases. This occurs because polarizability is proportional to volume, so that interaction energy between the electric field and the induced dipole increases with volume. The particle becomes fully aligned when the magnitude of the

interaction energy is significantly greater than the Brownian energy kT .

We also show that the ratio of fully aligned to random mobility is a function of the number of primary spheres and the primary sphere size. Near the continuum regime, the mobility ratio is approximately constant with N , and near the free molecule regime, the mobility ratio decreases with N . We discuss this topic in some detail in the SI, but the brief explanation is as follows: the mobility of an aggregate in the continuum and free molecule regimes is roughly inversely proportional to the radius of gyration (Meakin et al. 1985; Sorensen 2011; Corson et al. 2017b) and the orientation-averaged projected area (Zhang et al. 2012), respectively. Similarly, the continuum and free molecule aligned mobilities are correlated to the inverses of the radius of gyration about the major axis of the polarizability tensor (i.e., the z' -axis), $R_{gz'}$, and the projected area in the plane normal to the z' -axis, $PA_{z'}$ (see the SI). Averaged over 20 cases, the ratio $R_g/R_{gz'}$ is approximately constant (after accounting for the statistical fluctuations described above) with N , while $PA/PA_{z'}$ decreases with N , mirroring the trends in the mobility ratios in the continuum and free molecule limits.

4.2. Validity of our slow rotation assumption

Our calculations assume that Brownian rotation is slow compared to translational relaxation, i.e., the aggregates are in the slow rotation limit. To assess the validity of this assumption, we use our EKR method to determine the translational friction coefficient (ζ_h , the harmonic average of the eigenvalues of the friction tensor) and the minimum rotational diffusion coefficient (Corson et al. 2017c). Using these calculated friction and diffusion

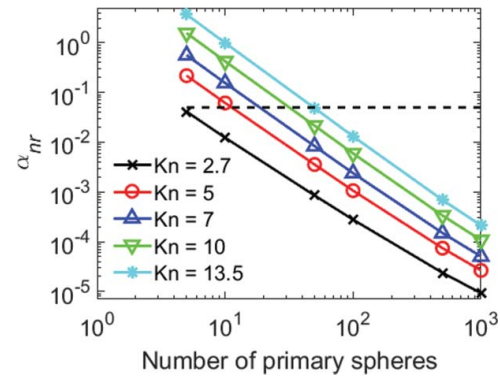


Figure 6. Reduced rotation velocity for a range of primary sphere sizes and Knudsen numbers. Soot density is taken as 2 g/mL, (Dobbins 2002; Park et al. 2004). Particles with a reduced rotation velocity less than 0.05 (the dotted line) are in the slow rotation limit.

³For a sample of n trials having a sample standard deviation s , the standard deviation of the mean is $\sigma_{\bar{x}} = s/\sqrt{n}$.

coefficients, we compute the reduced rotation velocity α_{nr} , as shown in Figure 6.

The figure shows that particles with Knudsen numbers less than 13.5 and more than approximately 50 primary spheres are in the slow rotation limit ($\alpha_{nr} < 0.05$; Mulholland et al. 2016); none of the particles in this study are in the fast rotation limit ($\alpha_{nr} > 10$). Note that for fast rotation, one should use an orientation-averaged drag approach to calculate the mobility, as opposed to the orientation-averaged drift velocity approach in the slow rotation limit. At low field strength, the fast rotation limit yields a scalar friction coefficient equal to the arithmetic average of the eigenvalues instead of the harmonic average in the slow rotation limit (Li et al. 2014a). (The two approaches yield the same result for the fully aligned case.) Thus, some of the particles included in this study are not in the slow rotation limit. However, the maximum difference between the mobility calculated using the averaged drift velocity is at most 1% less than the mobility calculated using the averaged drag force for the particles in this study (i.e., those with fractal dimensions of 1.78). In other words, it makes little difference which approach one uses to calculate the mobility of DLCA aggregates. The distinction becomes more significant for particles with a large aspect ratio, such as long, thin rods, where there is a large difference between the largest and smallest eigenvalues of the friction tensor.

4.3. Polarizability versus friction

A conducting particle in an electric field will orient itself to minimize its interaction energy with the field, in the absence of any Brownian thermal forces. The minimum energy occurs when the charge separation in the particle is greatest. This means that a rod or a chain of spheres will orient itself such that its long axis is parallel to the electric field, while the fractal particles in our study are oriented such that the axis through the most widely separated two spheres is parallel to the field. One would expect that the minimum drag force also occurs when it moves along its most elongated direction. This is exactly the case for axisymmetric particles like rods and cylinders, so that the most likely orientation of the particle in an electric field is the orientation with the minimum drag. For fractals, the situation is more complicated: there is a finite angle between the eigenvector of the friction tensor corresponding to the minimum drag and the principal axis of the polarizability tensor (the most favorable orientation). In most cases, this angle is small ($< 10^\circ$), though we have observed angles as large as 25° between these two eigenvectors. This means that the most favorable orientation does not necessarily minimize the drag for fractals.

A somewhat related issue is that translating particles with arbitrary shape experience a torque, where the relationship between the particle velocity and the torque exerted by the fluid on the particle is governed by the coupling tensor (Happel and Brenner 1965). For non-skew particles (such as rods and cylinders), there is no translational-rotational coupling, but for skew particles like fractals the coupling tensor is non-zero. The question is whether or not the hydrodynamic torque is sufficient to overcome the interaction energy between the induced dipole and the field and reorient the particle.

To answer this question, we calculated the coupling torque on 1000-sphere aggregates with a primary sphere Knudsen number of 13.5, using our EKR method to determine the coupling tensor (Corson et al. 2017c) and the orientation-averaged drift velocity at a field strength of 4000 V/cm (roughly corresponding to the minimum field strength at which the particle is fully aligned). The resulting torque is more than two orders of magnitude lower than the interaction energy. We repeated this calculation for $N = 100$, $Kn = 2.7$, and $E = 200$ V/cm; again, the coupling torque is significantly lower than the interaction energy. This shows that the coupling torque has no effect on the particle orientation at high field strength.⁴

4.4. Using field-dependent mobility to evaluate particle shape

Our results clearly show that particle mobility increases with electric field from a fully random state at low fields to a fully oriented state at higher fields. The transition occurs at decreasing fields for increasing particle size (both in terms of primary sphere size and the number of primaries), as expected since polarizability is proportional to particle volume.

This behavior has prompted some researchers to propose methods to separate particles with different shapes by exploiting the changes in mobility at different electric fields, such as by size-selecting particles in a DMA, followed by separation with second DMA operated at a different field strength (Zelenyuk and Imre 2007; Li et al. 2014b). Using this method, one can distinguish between spheres (or aggregates with

⁴At low field strength, translational-rotational coupling has a small but noticeable effect on the orientation-averaged drag force. For this reason, one must account for rotational and translation-rotation coupling effects when determining the translational diffusion of skew particles (Brenner 1967). To fully account for rotational and coupling effects at intermediate fields—where both hydrodynamic torques and induced-dipole energies affect particle orientation—one could use a Brownian approach similar to that of Fernandes and Garcia de la Torre (2002).

fractal dimension near 3) and more elongated particles like rods, chains, prolate ellipsoids, or soot-like aggregates, since the mobility of a sphere does not change with field strength. In practice, this technique may not be feasible for some particle sizes due to limitations of current commercially available DMA operating conditions and configurations. For example, Li et al. (2016) estimate that they cannot operate their experimental system at fields below 1000 V/cm. At this field strength, larger particles are fully aligned (see Figures 2 and 3), so measuring the mobility at fields of 1000 V/cm and e.g., 8000 V/cm would yield the same result and lead to the erroneous conclusion that the particle is spherical. At the other end of the size spectrum, small fractals experience minimal changes in mobility over the range of electric fields studied here. It may also be difficult to operate a DMA at a low enough field to ensure that the particle orientation is fully random. One can consult Figure 4 to determine if it is possible to select randomly oriented particles for the operating conditions of one's DMA setup.

There are also issues distinguishing between two nonspherical particles with different shapes. For example, the fully aligned mobility of a doublet in continuum flow is 8% greater than the mobility of a randomly oriented doublet (Happel and Brenner 1965; Carrasco and Garcia de la Torre 1999). This is comparable to the increase in mobility from random to fully aligned orientations for the soot particles included in our study. Thus, a doublet with primary size near the continuum regime and a soot-like particle with the same low-field mobility will behave similarly at higher voltages, making it difficult to distinguish between these particles. As another example, we looked at the effect of the prefactor (k_0 in Equation (17)) on the mobility of DLCA aggregates. While the prefactor does affect the mobility (with lower prefactors resulting in decreased mobility for the same number of primary spheres), it has little effect on the ratio of the fully aligned to fully random mobilities.

Beyond the experimental issues mentioned above, it is also difficult to accurately calculate the mobility of a fractal aggregate in the transition regime. We have estimated that our EKR method yields orientation-averaged translational friction coefficients within 10% of the true value (Corson et al. 2017b), which translates to uncertainties in any estimate of the primary sphere size or the number of primary spheres. An obvious example is our attempt to fit our results to the data of Li et al. (2016), as illustrated by Figure 1: our estimated aggregate sizes (in terms of N) are likely within about 10% of the true value

(though the actual error estimate depends on the relationship between N and the friction coefficient). This situation is simplified by the fact that we know the primary sphere size from transmission electron microscopy (TEM) measurements, and we have a good estimate of the fractal dimension and prefactor from numerous studies of soot. See (Sorensen 2011) for a review of these studies.

In total, the above factors mean that while it may be theoretically possible to extract shape information from DMA measurements made at different field strengths, it is difficult, and probably further consideration should be given to development of DMA configurations optimized for this purpose.

5. Conclusions

We have applied our EKR method for calculating the translational friction tensor of fractal aggregates to verify the theory of Li et al. (2014a) for the average mobility of a particle in an electric field. Our results compare well to published experimental data for soot (Li et al. 2016). Furthermore, we have used our EKR method to calculate the average mobility of aggregates over a range of primary sphere sizes in the transition and near-free molecule regimes with up to 2000 primary spheres. The maximum increase in mobility from random to fully aligned orientations is approximately 8% for the soot-like aggregates ($d_f = 1.78$, $k_0 = 1.3$) included in this study. While our calculations cover the Knudsen number range of 2.7–13.5—which covers a representative range of primary sphere sizes in soot particles (Koçylu and Faeth 1992; Li et al. 2016)—our approach is valid for any primary sphere size and number of primaries, provided the particle is in the slow rotation limit. (See Corson et al. [2017b,d] for translational and rotational friction coefficient results at larger and smaller Knudsen numbers.)

While it is theoretically possible to use the relationship between mobility and field strength to obtain size and shape information about particles or to separate particles with similar mobility but different shapes, our results suggest there are several practical issues related to the experimental setup and to the accuracy of the methods used to relate the data to size and shape information. It is especially difficult to obtain shape information for either very large or very small soot-like aggregates because large aggregates are fully aligned at even very low field strengths and small aggregates require very high field strengths to align. In these limits, the measured mobility at low (~ 1000 V/cm) and high (~ 8000 V/cm) field strengths would be nearly equal, which would suggest—incorrectly—that these fractal aggregates are actually spherical.

References

- Bhatnagar, P. L., Gross, E. P., and Krook, M. (1954). A Model for Collision Processes in Gases. I. Small Amplitude Processes in Charged and Neutral One-Component Systems. *Phys. Rev.*, 94(3):511–525. doi:10.1103/PhysRev.94.511.
- Bottcher, C. J. F., and Belle, O. C. V. (1973). *Dielectrics in Static Fields*. Elsevier Scientific Publishing Company, Amsterdam.
- Brenner, H. (1967). Coupling Between the Translational and Rotational Brownian Motions of Rigid Particles of Arbitrary Shape: II. General Theory. *J. Colloid Interface Sci.*, 23(3):407–436. doi:10.1016/0021-9797(67)90185-3.
- Carrasco, B., and Garcia de la Torre, J. (1999). Improved Hydrodynamic Interaction in Macromolecular Bead Models. *J. Chem. Phys.*, 111(10):4817–4826. doi:10.1063/1.479743.
- Chen, Z.-Y., Deutch, J. M., and Meakin, P. (1984). Translational Friction Coefficient of Diffusion Limited Aggregates. *J. Chem. Phys.*, 80(6):2982–2983. doi:10.1063/1.447012.
- Colbeck, I., Atkinson, B., and Johar, Y. (1997). The Morphology and Optical Properties of Soot Produced by Different Fuels. *J. Aerosol Sci.*, 28(5):715–723. doi:10.1016/S0021-8502(96)00466-1.
- Corson, J., Mulholland, G. W., and Zachariah, M. R. (2017a). Friction Factor for Aerosol Fractal Aggregates over the Entire Knudsen Range. *Phys. Rev. E*, 95(1):013103. doi:10.1103/PhysRevE.95.013103.
- Corson, J., Mulholland, G. W., and Zachariah, M. R. (2017b). Analytical Expression for the Friction Coefficient of DLCA Aggregates Based on Extended Kirkwood–Riseman Theory. *Aerosol Sci. Technol.*, 51(6):766–777. doi:10.1080/02786826.2017.1300635.
- Corson, J., Mulholland, G. W., and Zachariah, M. R. (2017c). Calculating the Rotational Friction Coefficient of Fractal Aerosol Particles in the Transition Regime using Extended Kirkwood–Riseman Theory. *Phys. Rev. E*, 96(1):013110. doi:10.1103/PhysRevE.96.013110.
- Corson, J., Mulholland, G. W., and Zachariah, M. R. (2017d). Analytical Expression for the Rotational Friction Coefficient of DLCA Aggregates over the Entire Knudsen Regime. *Aerosol Sci. Technol.*, 52(2):206–221. doi:10.1080/02786826.2017.1390544.
- Dobbins, R. A. (2002). Soot Inception Temperature and the Carbonization Rate of Precursor Particles. *Combust. Flame*, 130(3):204–214. doi:10.1016/S0010-2180(02)00374-7.
- Douglas, J. F., Zhou, H.-X., and Hubbard, J. B. (1994). Hydrodynamic Friction and the Capacitance of Arbitrarily Shaped Objects. *Phys. Rev. E*, 49(6):5319. doi:10.1103/PhysRevE.49.5319.
- Fernandes, M. X., and Garcia de la Torre, J., 2002. Brownian Dynamics Simulation of Rigid Particles of Arbitrary Shape in External Fields. *Biophys. J.*, 83(6):3039–3048. doi:10.1016/S0006-3495(02)75309-5.
- Fuchs, N. A., 1964. *The Mechanics of Aerosols*. Pergamon Press (distributed in the Western Hemisphere by Macmillan), New York, NY, pp. 245–249.
- Gel'fand, I. M., Minlos, R. A., and Shapiro, Z. Y. (1963). *Representations of the Rotation and Lorentz Groups and Their Applications*. Pergamon Press (distributed in the Western Hemisphere by Macmillan), New York, NY.
- Happel, J., and Brenner, H., 1965. *Low Reynolds Number Hydrodynamics: With Special Applications to Particulate Media*. Prentice Hall, Englewood Cliffs, NJ, pp. 159–235.
- Kirkwood, J. G., and Riseman, J. (1948). The Intrinsic Viscosities and Diffusion Constants of Flexible Macromolecules in Solution. *J. Chem. Phys.*, 16(6):565–573. doi:10.1063/1.1746947.
- Kousaka, Y., Endo, Y., Ichitsubo, H., and Alonso, M. (1996). Orientation-Specific Dynamic Shape Factors for Doublets and Triplets of Spheres in the Transition Regime. *Aerosol Sci. Technol.*, 24(1):36–44. doi:10.1080/02786829608965350.
- Koylu, U. O., and Faeth, G. M. (1992). Structure of Overfire Soot in Buoyant Turbulent Diffusion Flames at Long Residence Times. *Combust. Flame*, 89(2):140–156. doi:10.1016/0010-2180(92)90024-J.
- Law, W. S., and Loyalka, S. K. (1986). Motion of a Sphere in a Rarefied Gas. II. Role of Temperature Variation in the Knudsen Layer. *Phys. Fluids (1958-1988)*, 29(11):3886–3888. doi:10.1063/1.865773.
- Lea, K. C., and Loyalka, S. K. (1982). Motion of a Sphere in a Rarefied Gas. *Phys. Fluids*, 25(9):1550–1557. doi:10.1063/1.863943.
- Li, M., Mulholland, G. W., and Zachariah, M. R. (2012). The Effect of Orientation on the Mobility and Dynamic Shape Factor of Charged Axially Symmetric Particles in an Electric Field. *Aerosol Sci. Technol.*, 46(9):1035–1044. doi:10.1080/02786826.2012.686675.
- Li, M., Mulholland, G. W., and Zachariah, M. R. (2014a). Understanding the Mobility of Nonspherical Particles in the Free Molecular Regime. *Phys. Rev. E*, 89(2):022112. doi:10.1103/PhysRevE.89.022112.
- Li, M., Mulholland, G. W., and Zachariah, M. R. (2016). The Effect of Alignment on the Electric Mobility of Soot. *Aerosol Sci. Technol.*, 50(10):1003–1016. doi:10.1080/02786826.2016.1213789.
- Li, M., You, R., Mulholland, G. W., and Zachariah, M. R. (2014b). Development of a Pulsed-Field Differential Mobility Analyzer: A Method for Measuring Shape Parameters for Nonspherical Particles. *Aerosol Sci. Technol.*, 48(1):22–30. doi:10.1080/02786826.2013.850150.
- Mackowski, D. W. (2006). Monte Carlo Simulation of Hydrodynamic Drag and Thermophoresis of Fractal Aggregates of Spheres in the Free-Molecule Flow Regime. *J. Aerosol Sci.*, 37(3):242–259. doi:10.1016/j.jaerosci.2004.11.011.
- Mansfield, M. L., Douglas, J. F., and Garboczi, E. J. (2001). Intrinsic Viscosity and the Electrical Polarizability of Arbitrarily Shaped Objects. *Phys. Rev. E*, 64(6):061401. doi:10.1103/PhysRevE.64.061401.
- Meakin, P., Chen, Z.-Y., and Deutch, J. M. (1985). The Translational Friction Coefficient and Time Dependent Cluster Size Distribution of Three Dimensional Cluster–Cluster Aggregation. *J. Chem. Phys.*, 82(8):3786–3789. doi:10.1063/1.448890.
- Mulholland, G. W., Hagwood, C. R., Li, M., and Zachariah, M. R. (2016). Effect of Particle Rotation on the Drift Velocity for Nonspherical Aerosol Particles. *J. Aerosol Sci.*, 101:65–76. doi:10.1016/j.jaerosci.2016.04.004.
- Park, K., Kittelson, D. B., Zachariah, M. R., and McMurry, P. H. (2004). Measurement of Inherent Material Density of

- Nanoparticle Agglomerates. *J. Nanopart. Res.*, 6(2):267–272. doi:10.1023/B:NANO.0000034657.71309.e6.
- Rotne, J., and Prager, S. (1969). Variational Treatment of Hydrodynamic Interaction in Polymers. *J. Chem. Phys.*, 50 (11):4831–4837. doi:10.1063/1.1670977.
- Sorensen, C. M. (2011). The Mobility of Fractal Aggregates: A Review. *Aerosol Sci. Technol.*, 45(7):765–779. doi:10.1080/02786826.2011.560909.
- Weiss, R. E., Kapustin, V. N., and Hobbs, P. V. (1992). Chain-Aggregate Aerosols in Smoke from the Kuwait Oil Fires. *J. Geophys. Res.: Atmos.*, 97(D13):14527–14531. doi:10.1029/92JD01372.
- Yamakawa, H. (1970). Transport Properties of Polymer Chains in Dilute Solution: Hydrodynamic Interaction. *J. Chem. Phys.*, 53(1):436–443. doi:10.1063/1.1673799.
- Zelenyuk, A., and Imre, D. (2007). On the Effect of Particle Alignment in the DMA. *Aerosol Sci. Technol.*, 41(2):112–124. doi:10.1080/02786820601118380.
- Zhang, C., Thajudeen, T., Larriba, C., Schwartzentruber, T. E., and Hogan Jr., C. J. (2012). Determination of the Scalar Friction Factor for Nonspherical Particles and Aggregates across the Entire Knudsen Number Range by Direct Simulation Monte Carlo (DSMC). *Aerosol Sci. Technol.*, 46(10):1065–1078. doi:10.1080/02786826.2012.690543.